Available online at www.sciencedirect.com
ScienceDirect
Journal of Molecular Catalysis A: Chemical 283 (2008) 23–28
JOURNAL OF MOLECULAR CATALYSIS A: CHEMICAL
www.elsevier.com/locate/molcata

Influence of plasma spraying parameter on microstructure and photocatalytic properties of nanostructured TiO_2–Fe_3O_4 coating

Qinghe Yu, Chungen Zhou *, Xin Wang

Department of Materials Science and Engineering, Beijing University of Aeronautics and Astronautics, Beijing 100083, China

Received 19 July 2007; received in revised form 13 November 2007; accepted 1 December 2007
Available online 23 December 2007

Abstract

TiO_2–Fe_3O_4 coatings on transparent glasses were prepared by atmospheric plasma spraying (APS). As-sprayed TiO_2–Fe_3O_4 coatings consist of anatase TiO_2, rutile TiO_2, Fe_3O_4 and $FeTiO_3$. The grain size, rate of porosity and fractions of the anatase and $TiFeO_3$ phases in APS coatings were dependent on the process parameters. With an increase in plasma power, the content of anatase TiO_2 and the rate of porosity in the coatings were decreased while the content of the resultant $FeTiO_3$ phase and the grain size in the coating were increased. The coating condition of 500 A has the best photocatalytic efficiency and 600 A has the worst. The photocatalytic property of the APS TiO_2–Fe_3O_4 coatings was primarily dependent on synergistic effect of the fractions of $FeTiO_3$ and anatase phases.

Keywords: Plasma spraying; Photocatalytic property; TiO_2; Fe_3O_4

1. Introduction

Nano-TiO_2 materials have many unique properties, which are attractive to many researchers for various high performance applications. For example, TiO_2 is known to be the best photocatalyst in terms of its chemical stability, low cost and lack of toxins [1]. It can be used to decompose the organic pollutants and sterilize bacterium in the air. For such applications titania exhibits at least two disadvantages [1–9]: the electron can only be excited from the valence to the conduction band by ultraviolet light; the anatase phase has a tetragonal structure and from the viewpoint of thermodynamics it is a metastable phase. To solve these problems, adding some metal element or semiconductor is necessary. The additions such as Fe_3O_4, Pt, SnO_2, Al_2O_3 [10–13] were used to improve the photocatalytic properties. Ye et al. [10] have studied the photocatalytic activity and photo-absorption of plasma-sprayed TiO_2–Fe_3O_4 binary oxide coatings. The results showed that the TiO_2–Fe_3O_4 coatings consist of anatase, rutile, Fe_3O_4 and $FeTiO_3$, and the content of anatase TiO_2 was estimated to be approximately 4%, which is lower than that of TiO_2 coatings from 8% to 15%. The addition of Fe_3O_4 can enhance the photocatalytic activity for the formation of $FeTiO_3$ compound in the TiO_2–Fe_3O_4 coatings. The photocatalytic activity of the TiO_2–Fe_3O_4 coating is related to the porosity, grain size and the content of the anatase phase and $FeTiO_3$ compound in the TiO_2–Fe_3O_4 coating. However, influence of atmospheric plasma spraying parameters on the porosity, grain size and the content of anatase phase and $FeTiO_3$ compound in the TiO_2–Fe_3O_4 coating have not been investigated extensively. With the above background, in the present investigation, influence of atmospheric plasma spraying parameters on the porosity, grain size and the content of the anatase phase and $FeTiO_3$ compound in the TiO_2–Fe_3O_4 coating, and the relationship between the process parameters of the APS process and TiO_2–Fe_3O_4 coating photo-decomposition efficiency have been explored. In addition, the photocatalytic mechanism of doped Fe_3O_4 was explained through TEM image.

2. Experimental procedures

2.1. Powder preparation

The original powder is composed of nearly 99.99% anatase TiO_2 (HTTi-01, Nanjing high technology nano company of

* Corresponding author. Tel.: +86 10 82338622; fax: +86 10 82338200.
E-mail address: cgzhou@buaa.edu.cn (C. Zhou).

1381-1169/$ – see front matter © 2007 Elsevier B.V. All rights reserved.
doi:10.1016/j.molcata.2007.12.011

China), which has a specific surface area of 120 m^2/g. TiO_2 average particle size is 5 nm, the Fe_3O_4 average particle size is 30 nm. The individual nano-particle is so fine that cannot be used for plasma spray. It is difficult to keep grain size at the nanometer regime in the coating, which may be achievable through the opportunities provided by using nano-sized particles, during the plasma spray, the particle size between 30 μm and 50 μm has the best fluidity. Before spraying finely dispersed particles of the material must be agglomerated to size about 30–50 μm. A particle size distribution around 50 μm was used in this study.

2.2. Coating preparation and characterization

2.2.1. Plasma spray

The powder diameter around 50 μm was plasma sprayed with a GP-80 high energy plasma spraying equipment in an opened room using hand-worked operation system. The powder feeding system was an integrative apparatus with controller system. The powder feed rate was fixed at 30 g/min. The transparent glass (1 mm × 76 mm × 26 mm) was used as substrate. Table 1 shows plasma spraying parameters for preparation of the nano-TiO_2–Fe_3O_4.

2.2.2. Photocatalytic properties

The schematic of the glass-plate photoreactor is shown in Refs. [14,15]. The procedure for all the experiments were as follows: (1) airflow was started; (2) after the photoreactor

Table 1
Condition for the APS deposition of the coatings in this study

Volts (V)	60
Current (A)	300, 400, 500, 600
Argon gas (L/min)	60
Hydrogen gas (L/min)	30
Powder feed rate (g/min)	30

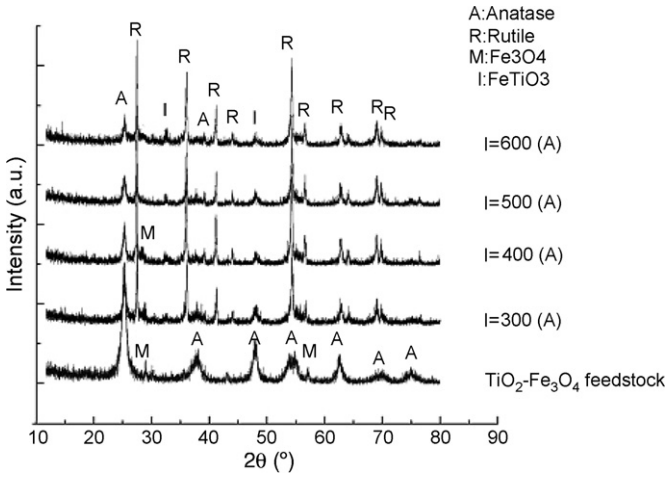

Fig. 1. X-ray diffraction patterns of TiO_2–Fe_3O_4 coatings.

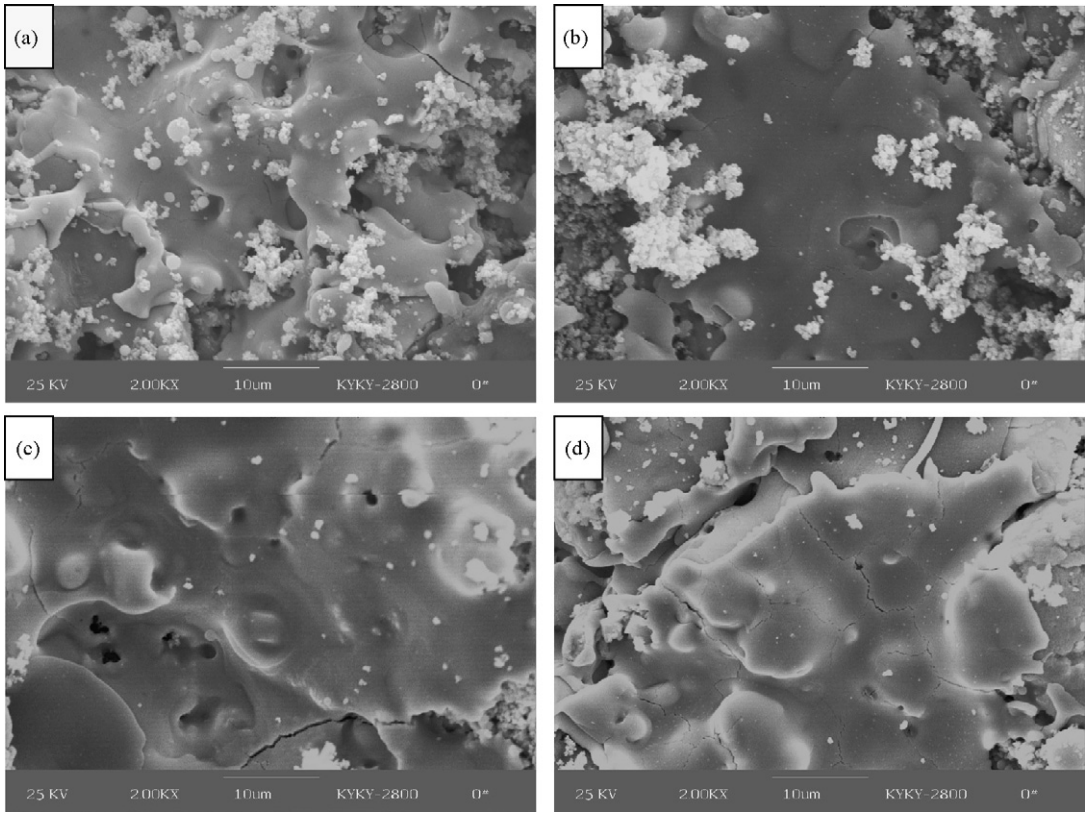

Fig. 2. Surface SEM of plasma spraying TiO_2–Fe_3O_4 coatings under current 300 A (a), 400 A (b), 500 A (c) and 600 A (d).

Table 2
The operating parameters for light-in-tube PCO reactor

Parameter	Value
Tested VOCs	Formaldehyde
Room temperature (K)	298
Initial concentration of VOCs C_{ini} (mg m^{-3})	1.35
Air volumetric flow rate G (m^3 h^{-1})	30
Volume of test chamber V (m^3)	1.73
Air of photocatalytic surface A (m^2)	0.002
UV-light wavelength (nm)	254

inlet and outlet humidity readings were steady and equal, the toluene was introduced; (3) when the photoreactor inlet and outlet toluene concentrations were approximately equal, the UV lamps were turned on; (4) after the inlet and outlet toluene levels again reached steady state, the UV lamps were turned off and the toluene flow was stopped; (5) the photoreactor was flushed with the synthetic air for 15 min, and then airflow was stopped.

Table 2 shows the operating parameters for light-in-tube PCO reactor coated with plasma-sprayed TiO_2–Fe_3O_4 powders.

2.2.3. Analytical techniques

The microstructure and phase characterization of the sprayed coatings were performed by means of X-ray diffraction (XRD), which use Cu target, 40 kV, 40 mA.

The KYKY-2800 type of scanning electron microscopy (SEM) made in China was used to observe the surface morphologies of the coatings. Particle morphology observation and crystal structure determination were also performed on an analytical transmission electron microscope (TEM). The porosity of TiO_2–Fe_3O_4 coatings was tested by mercury porosimetry method, using AUTOPORE II 9220 V3.04, which is made by Micromeritics Inc., USA.

3. Experimental results

3.1. Microstructures of the sprayed TiO_2–Fe_3O_4 coatings

As shown in Fig. 1, the sprayed TiO_2–Fe_3O_4 coatings mainly consist of rutile phase, anatase phase and iron titanium oxide ($FeTiO_3$). Some of the anatase phase transformed to a stable rutile phase during thermal spraying process. Through the fol-

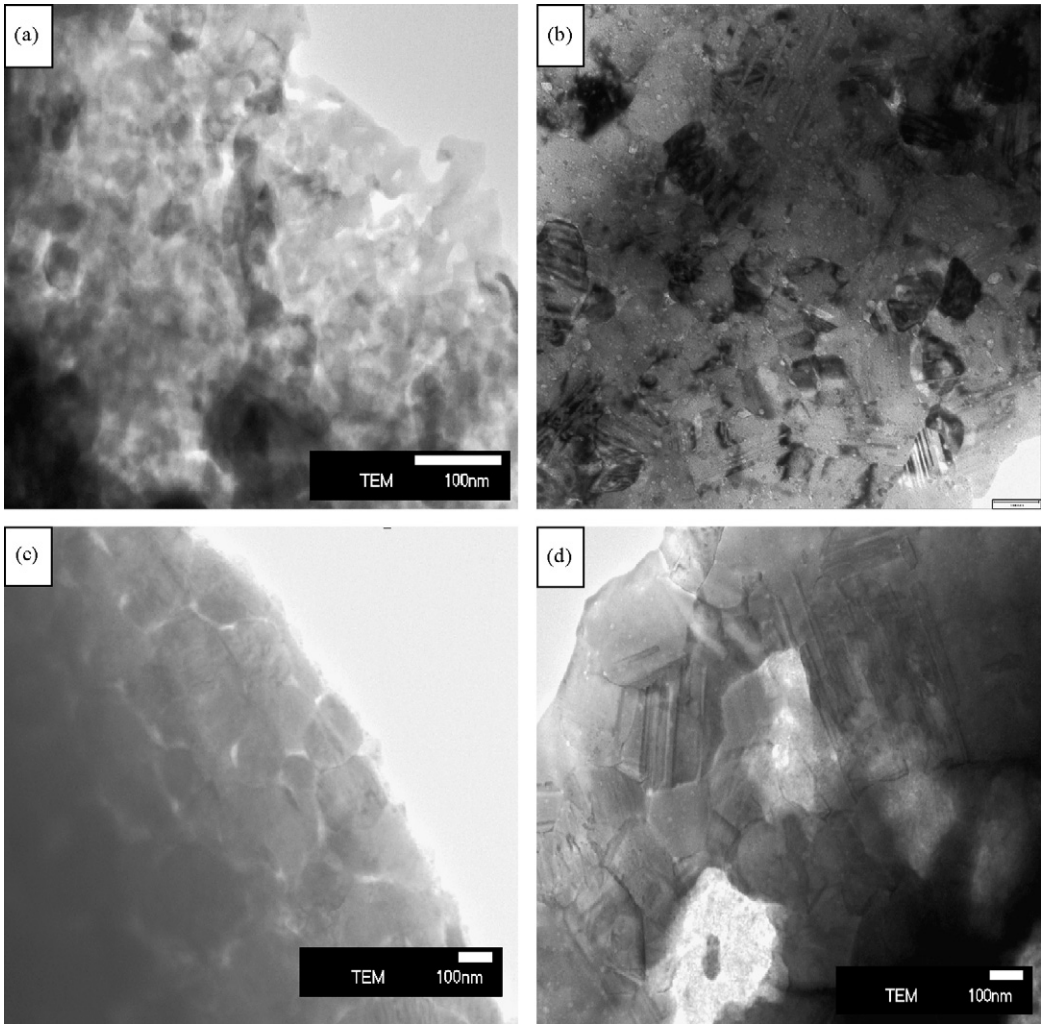

Fig. 3. TEM image of plasma-sprayed TiO_2–Fe_3O_4 coatings 300 A (a), 400 A (b), 500 A (c) and 600 A (d).

lowing equation [16]:

$$A = \frac{1}{(1 + 1.265 I_R / I_A)} \quad (1)$$

where I_A is the highest peak intensity of anatase phase, I_R is the highest peak intensity of rutile phase; A is the content of anatase TiO_2 in the coatings. The content of the anatase is calculated to be about 20.7%, 19.2%, 17.5% and 15.2% under the current of 300 A, 400 A, 500 A and 600 A, respectively. It is also seen from Fig. 1 that with the increasing current, the content of the resultant phase $FeTiO_3$ is increased. During the plasma spraying, the following reaction can take place:

$$TiO_2 + Fe_3O_4 \rightarrow FeTiO_3 \quad (2)$$

Under the conditions of 300 A and 400 A, there is still Fe_3O_4 phase left after spraying. However, there is no Fe_3O_4 remnant in the coating after spraying at the current of 500 A and 600 A. This result indicates that Fe_3O_4 reacted with TiO_2 completely due to the higher spraying temperature, and all the Fe_3O_4 particles changed into $FeTiO_3$.

Fig. 2 presents the SEM of the plasma-sprayed coatings which shows the typical surface microstructures of TiO_2–Fe_3O_4 coatings with 300 A (a), 400 A (b), 500 A (c) and 600 A (d). The TiO_2–Fe_3O_4 coatings are not very dense; contain many holes and cracks. It also can be seen that there are two kinds of structures in the coating. One is the continuous molten phase, and the other is the loose microstructure, which resulted from the existence of the non-molten or semi-molten starting powders. During the plasma spraying, the working fluid (plasma flame)

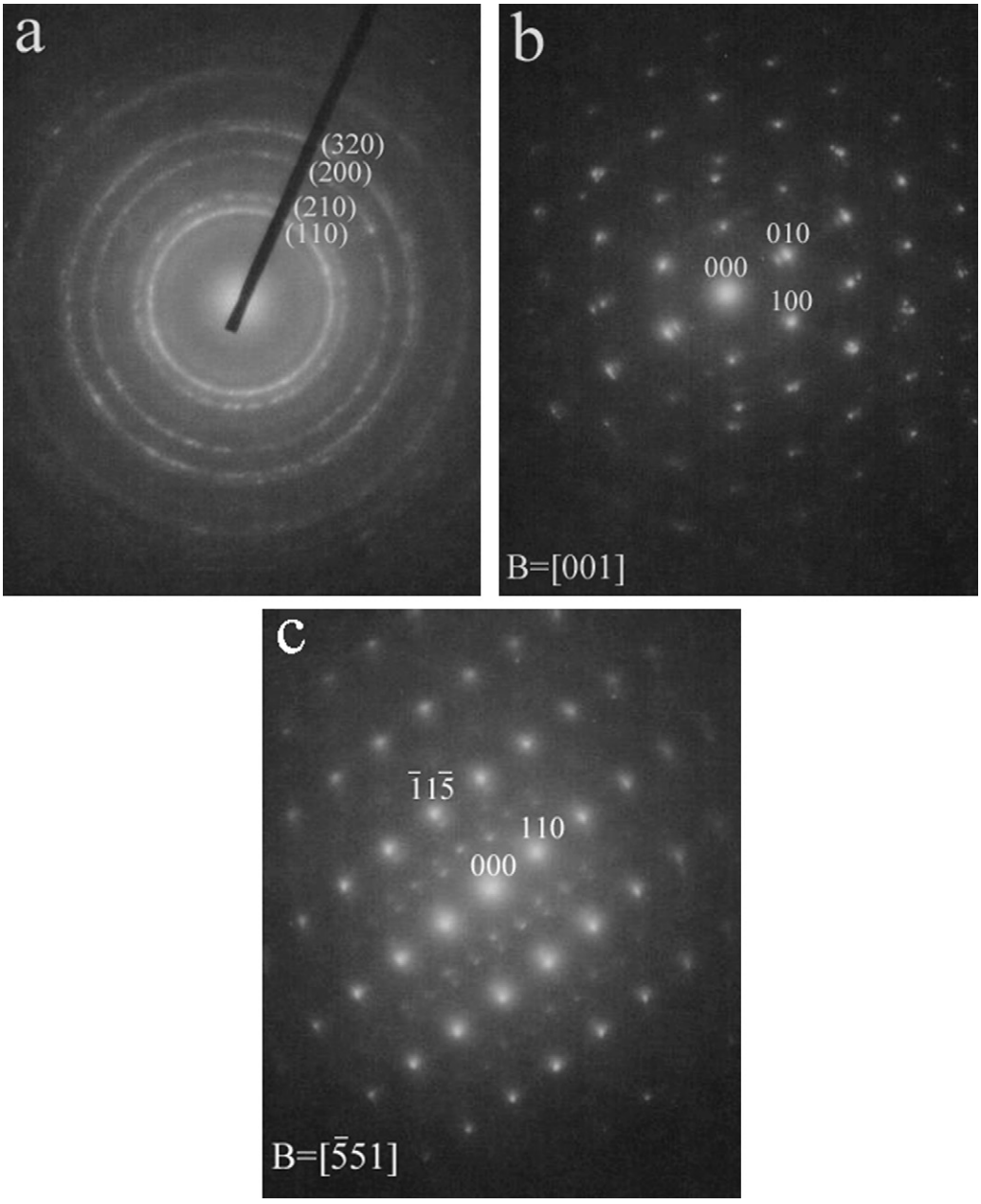

Fig. 4. The selected area electron diffraction patterns (SAEDPs) of as-sprayed TiO_2–Fe_3O_4 coatings.

has a high enthalpy density [6], which is controlled by the arc current conditions. The larger current offers a higher enthalpy density, which induces the different melting phenomena of starting powders. The low melting point (approx. 1873 K) of the added Fe_3O_4 [10] also induces the different melting phenomena. The TiO_2–Fe_3O_4 powders melted more fully with the increasing current. The partly and unmelted particles exist is a kind of phenomenon which will be a benefit to increase the specific surface and then improve the photocatalytic activity of the sprayed coatings [18]. Coatings with many holes and cracks also have an important influence on the photocatalytic activity.

Fig. 3 presents the typical TEM morphologies of the plasma-sprayed TiO_2–Fe_3O_4 coatings under different current conditions. From the comparison among 300 A (a), 400 A (b), 500 A(c) and 600 A (d), we can get that with the increasing current, the grain size growing up gradually. The grain size is about 20 nm, 40 nm, 60 nm and 100 nm corresponding to 300 A, 400 A, 500 A and 600 A current conditions. A large grain size has a small specific surface area.

Fig. 4 shows the selected area electron diffraction patterns (SAEDPs) of APS TiO_2–Fe_3O_4 coatings. By the calculation of the indices of crystallographic plane, the polycrystalline diffraction ring of TiO_2 obtained is shown in Fig. 4(a). As confirmed by the SAEDP, the TiO_2–Fe_3O_4 coatings is primarily composed of $FeTiO_3$ phase by using [0 0 1] and [$\bar{5}$ 5 1] zone axes, respectively. The calculated result is shown in Fig. 4(b) and (c). The Fe_3O_4 phase does not occur in the selected area electron diffraction patterns of APS TiO_2–Fe_3O_4 coatings, which clearly indicates that $FeTiO_3$ phase directly influences the photocatalytic property of the coating. The new $FeTiO_3$ phase has a great important influence on the photocatalytic property. $FeTiO_3$ phase not only can make use of long wavelength, but also can inhibit the recombination of holes and electrons.

3.2. Rate of porosity and photo-characteristics

Fig. 5 shows the variation of the rate of porosity with the current. When the current is 400 A, it has the highest rate of porosity. But when the arc current gets to 500 A and 600 A, the thermal enthalpy is so high that the coating becomes dense and has a low porosity as shown in Fig. 5. If the coating has a high rate of porosity, it has a better absorption, which may lead to a better photocatalytic property.

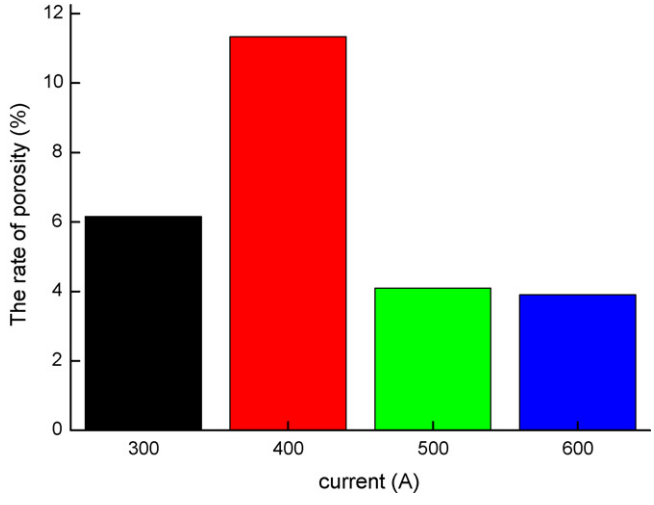

Fig. 5. Variation of the TiO_2–Fe_3O_4 coatings rate of porosity with the current.

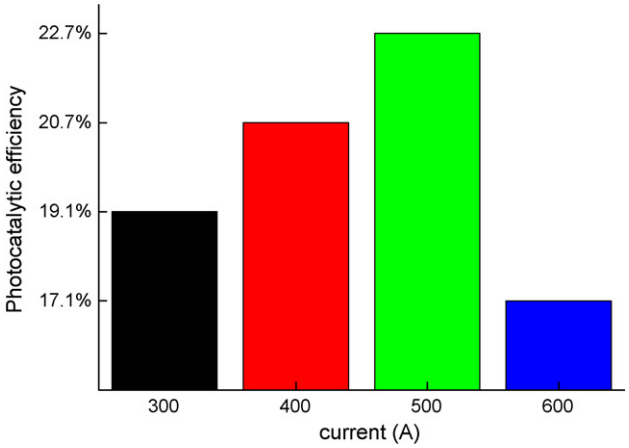

Fig. 6. Variation of the TiO_2–Fe_3O_4 coatings photocatalytic efficiency with the current.

Fig. 6 shows the variation of the TiO_2–Fe_3O_4 coatings photocatalytic efficiency with the spraying current. The coating condition of 500 A has the best photocatalytic efficiency, while 600 A has the worst. With the arc current increasing, photocatalytic efficiency is increased first and then decreased.

As shown in the above results, the coating condition of 300 A has a higher anatase fraction and finer grain size for its low current. At the current of 400 A, it has a higher rate of porosity compared with other current conditions. Although the coating condition of 500 A had a larger grain size, lower content of anatase phase, lower rate of porosity than that of 300 A and 400 A conditions, its photo-decomposition efficiency was still better than the case of 300 A and 400 A. The reason may be as follow: when the current arrives to 500 A or 600 A, TiO_2 reacted with Fe_3O_4 completely, all the Fe_3O_4 particles changed into $FeTiO_3$. The forbidden band gap of new phase $FeTiO_3$ is 2.58 eV [17], less than the anatase forbidden gap 3.2 eV [1,10]. The $FeTiO_3$ phase as a medium mediator could receive the electrons initiated from value band of TiO_2; consequently inhibit the recombination of the electrons and holes [19,20,22]. The narrow band gap could absorb light of longer wavelength, consequently improving the photocatalytic property. Therefore, it seems that the content of the $FeTiO_3$ phase and anatase phase played a synergistic effect (inhibiting the recombination of the electrons and holes) in the process of photo-decomposition. The synergistic effect is a more dominant factor than the grain size and the rate of porosity. The content of the $FeTiO_3$ phase obtained at the current of 600 A is almost the same as that at the current of 500 A, but the coating condition of 600 A has lower anatase fraction, larger grain size and lower rate of porosity than 500 A; the content of $FeTiO_3$ phase is higher than that of 300 A and 400 A. However, there is lower content of anatase phase and higher content of rutile phase in the coating. Therefore, the synergistic effect is weaker compared to the other current conditions. Moreover, photocatalytic

property of $FeTiO_3$ phase and content of anatase phases are very low, and, resulting in the coating condition of 600 A has the lowest photocatalytic efficiency. Considering all these conditions, the coating condition of 500 A has the best photocatalytic property. Changhoon Lee et al. [1,5,20,21] investigated single factor such as the grain size and porosity on photocatalytic property. It is evident that the coating with a higher porosity and a smaller grain size shows a greater effective photo-decomposition. Ye et al. [8,10,22] studied the influence of Fe_3O_4 on photocatalytic property. The photocatalytic activity was improved with an increase of $FeTiO_3$ content in the coating, which was explained by the good photoabsorbance capacity and by the two-step electron transfer model. Although single factor on photocatalytic property has been investigated, combined effects of the content of $FeTiO_3$ and anatase phases, grain size and rate of porosity on the photocatalytic property of the APS TiO_2–Fe_3O_4 coatings need to be investigated in the future study.

4. Conclusions

TiO_2–Fe_3O_4 coatings were deposited on glass substrates by plasma spraying. As-sprayed TiO_2–Fe_3O_4 coatings is composed of anatase, rutile, Fe_3O_4 and $FeTiO_3$. With an increase in plasma power, the content of anatase TiO_2 was decreased and the rate of porosity first went up and then dropped in the coatings, the content of the resultant $FeTiO_3$ phase and the grain size in the coating were increased. The photocatalytic property of the APS TiO_2–Fe_3O_4 coatings was primarily dependent on synergistic effect of the fractions of $FeTiO_3$ and anatase phases.

Acknowledgements

This work is supported by the National Natural Science Foundation of China under the contact 50436040, Program for New Century Excellent Talents in University (NCET) and Program for Changjiang Scholars and Innovative Research Team in University (PCSIRT) (IRT0512).

References

[1] C. Lee, H. Choi, C. Lee, et al., Surf. Coat. Technol. 173 (2003) 192.
[2] J. Yu, X. Zhao, Q. Zhao, Mater. Chem. Phys. 69 (2001) 25.
[3] Q. Fang, J.Y. Zhang, Z.M. Wang, et al., Thin Solid Films 428 (2003) 263.
[4] Yu.V. Kolen'ko, B.R. Churagulov, M. Kunst, et al., Appl. Catal. B: Environ. 54 (2004) 51.
[5] N. Berger-Keller, G. Bertrand, C. Filiatre, et al., Surf. Coat. Technol. 168 (2003) 281.
[6] J. Karthikeyan, C.C. Berndt, J. Tikkanen, et al., Mater. Sci. Eng. A 238 (1997) 275.
[7] L.L. Shaw, D. Goberman, R. Ren, et al., Surf. Coat. Technol. 130 (2000) 1.
[8] F. Ye, A. Ohomio, Trans. Nonferrous Met. Soc. China 114 (2) (2004) 55.
[9] S. Beauvais, V. Guipont, F. Borit, et al., Surf. Coat. Technol. 183 (2004) 204.
[10] F. Ye, A. Ohmori, Surf. Coat. Technol. 160 (2002) 62.
[11] A.I. Martínez, D.R. Acosta, G. Cedillo, Thin Solid Films 490 (2005) 118.
[12] E. Celik, I. Keskin, I. Kayatekin, et al., Mater. Charact. 58 (2007) 349.
[13] W. Teoh, L. Mäler, D. Beydoun, et al., Chem. Eng. Sci. 60 (2005) 5852.
[14] R. Yang, Y. Zhang, R. Zhao, J. Air Waste Manage. Assoc. 54 (2004) 1516.
[15] R. Yang, Y. Zhang, Q. Xu, Atmos. Environ. 41 (2007) 1221.
[16] R.A. Spurr, H. Myers, Anal. Chem. 29 (5) (1957) 760.
[17] D.S. Ginley, M.A. Butler, J. Appl. Phys. 48 (5) (1977) 2019.
[18] Y. Zeng, J.T. Liu, W. Wu, et al., Surf. Coat. Technol. 200 (2005) 2398.
[19] R. Alexandrescu, I. Morjan, M. Scarisoreanu, et al., Thin Solid Films 515 (2007) 8438.
[20] M.C. Hidalgo, M. Maicu, J.A. Navío, et al., Catal. Today 129 (2007) 43.
[21] D.S. Kim, S.J. Han, S.Y. Kwak, J. Colloid Interface Sci. 316 (2007) 85.
[22] F.X. Ye, T. Tsumura, K. Nakata, et al., Mater. Sci. Eng. B 148 (2008) 154.